RESOURCE GEOLOGY

doi: 10.1111/rge.12124 *Resource Geology* Vol. 67, No. 2: 139–157

Original Article

Geochemical Characterization of Magnetite and Geological Setting of the Iron Oxide ± Iron Silicate ± Iron Carbonate Rich Pb–Zn Sulfides from the La Unión and Mazarrón Stratabound Deposits (SE Spain)

José Ángel López-García,[1] Roberto Oyarzun,[1,2] Javier Lillo,[2,3] José Ignacio Manteca[4] and Paloma Cubas[2,5]

[1]*Departamento de Cristalografía y Mineralogía, Facultad de Ciencias Geológicas, and* [5]*Biología Vegetal II, Facultad de Farmacia, Universidad Complutense, Madrid,* [2]*Instituto de Geología Aplicada (IGeA), Universidad de Castilla-La Mancha, Ciudad Real,* [4]*Departamento de Ingeniería Minera, Geológica y Cartográfica, Universidad Politécnica de Cartagena, Cartagena and* [3]*Escuela Superior de Ciencias Experimentales y Tecnología, Universidad Rey Juan Carlos, Móstoles, Madrid, Spain*

Abstract

From a mineralogical point of view the La Unión ore field (SE Spain) can be regarded as an oddity as some of its hydrothermal, stratabound type deposits display an extremely unusual paragenesis comprising magnetite ± greenalite ± minnesotaite ± siderite and galena ± sphalerite (IOSC – LZS). Recent mineralogical studies have shown that this paragenesis is also present at the neighboring Mazarrón ore field. These ore fields share a similar geologic setting, involving metamorphic and sedimentary rocks (Paleozoic *s.l.* to Permian) hosting late Miocene high-K calc-alkaline volcanic and subvolcanic rocks. The latter have andesitic to dacitic composition, and triggered hydrothermal activity and ore deposition. This study discusses the detailed mineral chemistry of magnetite samples from Mazarrón and La Unión and provides some hints for the origin of the IOSC – LZS paragenesis. We performed electron microprobe (EPMA) analyses in magnetite samples from La Unión and Mazarrón to determine the contents of minor and trace elements (Zn, Ni, Mn, Cr, V, K, Ca, Ti, Al, Si, Mg). Given that some results fell below the detection limit for the EPMA instrumental conditions we used robust regression on order statistics (robust ROS), with the NADA package in R to deal with these data sets. The Ca + Al + Mn contents in magnetites from San Cristóbal and Emilia are equivalent to the mean contents of those of IOCG, Kiruna, BIF, Cu porphyry, skarn, VMS, hydrothermal and clastic Pb–Zn deposits, but they are low in Ti + V and Ni + Cr. The principal components analysis indicates that Zn, Ni, Cr, V, K, Ca, Ti, and Mg are roughly collinear, therefore correlated, being also independent from Fe. Besides, the function discriminant analysis of data shows that the magnetites from Emilia and San Cristóbal cluster in differentiated groups, thus probably reflecting some differences related to the distance to the magmatic source that triggered the hydrothermal system: proximal in the case of San Cristóbal and distal in Emilia.

Keywords: High-K calc-alkaline magmatism, magnetite, mineral chemistry, Miocene, Pb–Zn–Fe ore deposits, SE Spain.

Received 1 February 2016. Revised 5 September 2016. Accepted for publication 6 October 2016.
Corresponding author: J.A. López-García, Departamento de Cristalografía y Mineralogía, Facultad de Ciencias Geológicas, Universidad Complutense, 28040 Madrid, Spain. Email: jangel@ucm.es

Introduction

This work is focused on two remarkable volcanic related, hydrothermal Pb–Zn ore fields defining the so called La Unión and Mazarrón ore fields, which are located in the NE tip of the 160 km long Cabo de Gata–Cartagena Volcanic Belt (ACVB) (e.g., Oyarzun *et al.*, 1995; López-García *et al.*, 2011) (Fig. 1). The unusual and remarkable presence of magnetite, iron silicates and iron carbonates together with Pb–Zn sulfides in Mazarrón and La Unión allows definition of an iron oxide + iron silicate + iron carbonate + Pb–Zn sulfides mineral parageneses (IOSC–LZS for short). Although the presence of these minerals was well known at La Unión (e.g., Pavillon, 1969; Oen *et al.*, 1975; Manteca & Ovejero, 1992), nothing had been published on this matter about Mazarrón until 2015, when a paper on sulfur isotopes (Esteban-Arispe *et al.*, 2015) (Fig. 2) brought up some information regarding one of the mineral parageneses of the ore field. However, no work on the mineral chemistry of the magnetite mineral phase has ever been published.

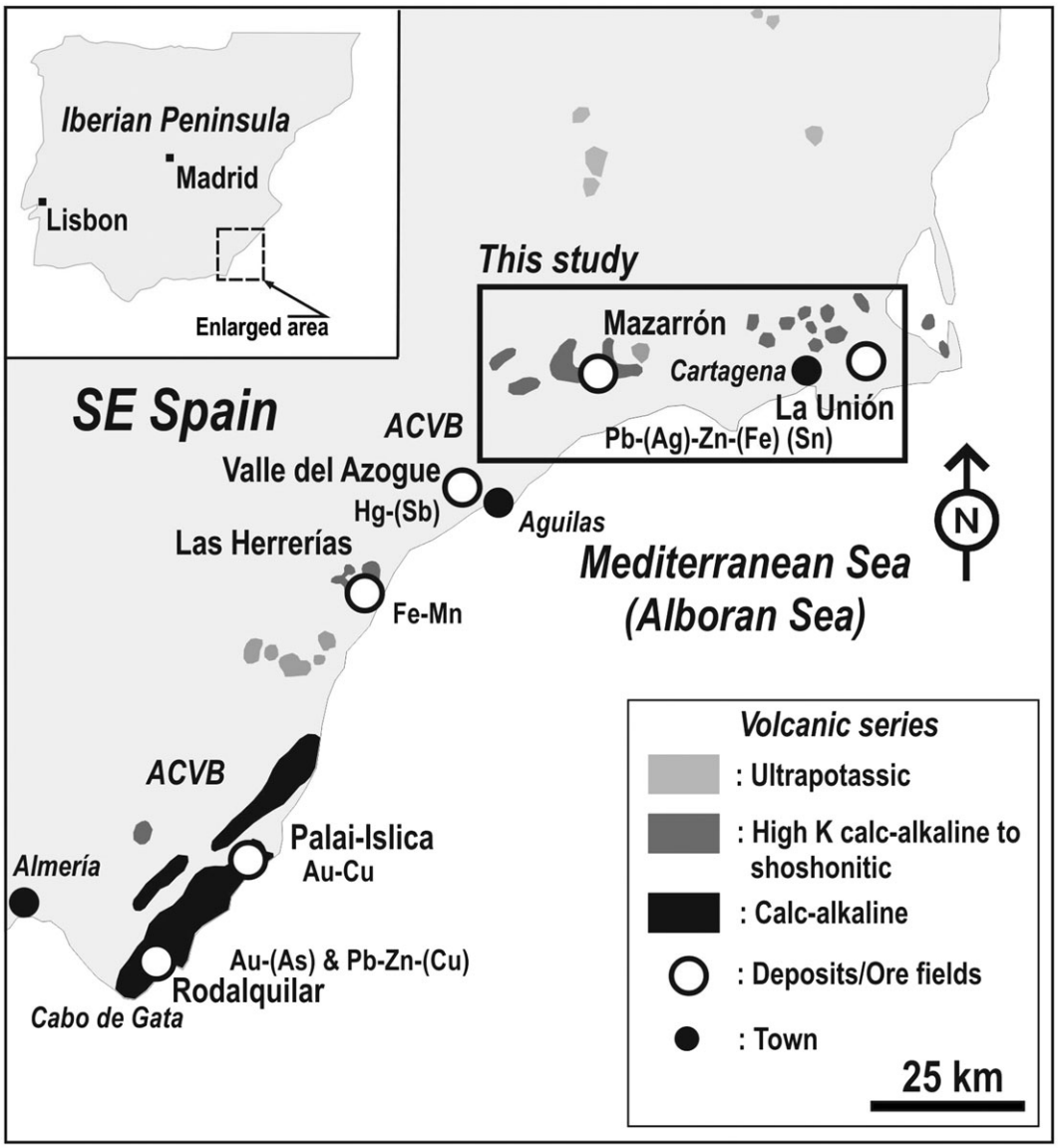

Fig. 1 The Cabo de Gata–Cartagena Volcanic Belt (ACVB) and main ore fields and volcanic series. Based on López-Ruiz and Rodríguez-Badiola (1980) and López-García *et al.* (2011). See inlet for location of the study zone.

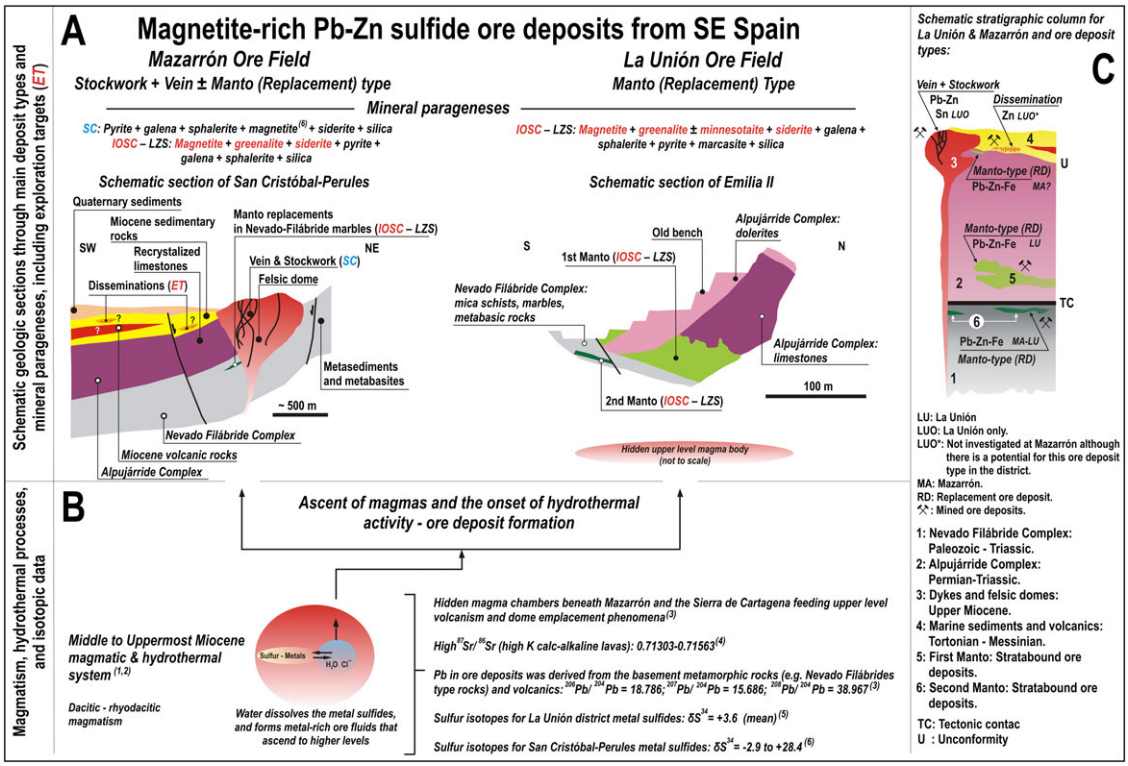

Fig. 2 Summary of main geologic, mineralogic and isotopic traits of representative ore deposits from Mazarrón and La Unión. (A) Schematic sections and mineral parageneses from San Cristóbal (Mazarrón) and Emilia II (La Unión) also depicting potential (district-scale) exploration targets; SC, sulfides + carbonates; IOSC–LZS, iron oxide, iron silicate, iron carbonate – lead and zinc sulfides. (B) Magma emplacement phenomena and hydrothermal transport of metals including the main isotopic signatures of rocks, lead, and sulfur; [1] Scaillet (2010); [2] Crespo *et al.* (2013); [3] Arribas and Tosdal (1994); [4] Benito *et al.* (1999); [5] Friedrich *et al.* (1964); [6] Esteban-Arispe *et al.* (2015). (C) Schematic and combined stratigraphic column (depicting ore deposits) for the La Unión and Mazarrón ore fields (not to scale).

This concise study aims: (i) to show the geological setting and mineralogical peculiarities of an odd and unique paragenetic mineral association characterized by the presence of an iron oxide ± iron silicate ± iron carbonate + Pb–Zn sulfides; and (ii) to show for the first time the chemical characteristics (minor and trace elements) of the magnetite mineral phase of two deposits from the La Unión (Emilia) and Mazarrón (San Cristóbal) ore fields (Figs 1, 2). The latter objective was also aimed to compare the geochemical data from Emilia and San Cristóbal with those from other ore deposits types (e.g., IOCG, porphyry, BIF) to assess whether they shared common geochemical features. We did 54 micro analyses in magnetites from Emilia and San Cristóbal for Zn, Ni, Mn, Cr, V, K, Ca, Ti, Al, Si, Mg, Fe, and dealt statistically with the chemical data via multivariate analyses. We show a concise scheme of the most relevant geological and mineralogical features (Fig. 2a), isotopic data (Fig. 2b), and stratigraphic relationships (Fig. 2c) of the ore fields hosting the Emilia and San Cristóbal deposits.

Tectonomagmatic and metallogenic setting

A brief account of the tectonic and magmatic evolution

The region (Betic Ranges) is characterized by the presence of the two most important Alpine metamorphic complexes (large-scale tectonic nappes) of SE Spain: Alpujárride (mainly limestones, dolomites, phyllites, and scattered intercalations of mafic rocks); and Nevado Filábride (mainly gneisses, mica schists, and metabasites), that were intensively folded during the late Oligocene–early Miocene. This realm subsequently underwent unroofing and volcanism in the Middle to Upper Miocene during a major extensional

event (Doblas & Oyarzun, 1989; Arribas, 1995; Benito *et al.*, 1999). Volcanism eventually led to formation of the present SW–NE trending coastal Miocene belt of SE Spain, that comprises a variety of volcanic series ranging from calc-alkaline (12–7 Ma), high-K calc-alkaline, and shoshonitic (12–6 Ma) rocks (e.g., López-Ruiz & Rodríguez-Badiola, 1980; Benito *et al.*, 1999; among others). The belt also hosts scattered outcrops of ultrapotassic rocks (8–6 Ma; e.g., Benito *et al.*, 1999) (Fig. 1) that did not play any role in ore forming processes (Oyarzun *et al.*, 1995). The calc-alkaline (CA) rocks are represented by basaltic andesites, pyroxene- and amphibole-bearing andesites and dacites; the mafic types have magnetite whereas the more evolved, felsic types bear both magnetite and ilmenite. The high-K calc-alkaline (HKCA) rocks (Fig. 1) include high-K andesites and dacites, whereas the shoshonitic (SH) series comprise banakites and latites; with some minor differences their mineralogy is similar to their equivalents of the CA series (Benito *et al.*, 1999). These rocks can be regarded as belonging to the magnetite series of Ishihara (1977, 2007), however, there is a transitional character in metallogenic terms as exemplified by the presence of Sn mineralization at the NE tip of the belt (the La Crisoleja ore deposit at the La Unión ore field) (Figs 1, 2c). In this regard, the negligible negative Eu anomaly in the CA and HKCA magmas (Benito *et al.*, 1999) suggests that oxygen fugacity must have been rather high (e.g., Coleman & Walker, 1990); therefore, despite the presence of Sn at La Unión (Fig. 2c) the magmas must be fully regarded as equivalent to those of the oxidized magnetite series magmas of Ishihara (1977). On the other hand, the Cabo de Gata–Cartagena belt (Fig. 1) is not the result of typical subduction-related processes (Doblas & Oyarzun, 1989; Arribas, 1995; Oyarzun *et al.*, 1995), but as a magmatic activity that developed in response to the massive extensional collapse of an overthickened Betic orogen (Alpine Orogeny) in SE Spain. This occurred through extensional detachment systems that induced major lithospheric stretching, asymmetric isostatic uprise of asthenospheric mantle towards the low-pressure thinned region, and eventually volcanism (Doblas & Oyarzun, 1989).

Ore deposits along the belt

The volcanic activity along the Cabo de Gata – Cartagena Belt triggered hydrothermal activity that led to formation of ore fields of the epithermal type; these encompass a variety of ore deposits types including those of Rodalquilar (Au, Pb–Zn–Cu), Palai-Islica (Au–Cu), Las Herrerías (Fe–Mn) or Valle de Azogue (Hg–Sb) (Arribas, 1995; Arribas *et al.*, 1995; Oyarzun *et al.*, 1995; Viladevall *et al.*, 1999; Morales Ruano *et al.*, 2000; López-García *et al.*, 2011; Oyarzun *et al.*, 2013) (Fig. 1). In this context La Unión and Mazarrón stand apart from the rest of the ore fields because some of their deposits are Pb–Zn–magnetite rich, thus defining a small and yet remarkable E–W oriented metallogenic domain (Fig. 1) that aside from magnetite also incorporates iron silicates and iron carbonates in a substantial proportion (IOSC–LZS).

As pointed out by Nadoll *et al.* (2014) magnetite is a common accessory mineral in host rocks, but a rare one in Pb–Zn hydrothermal ores; besides, as derived from their work and that from the study of Dupuis and Beaudoin (2011), magnetite only occurs as a minor or trace mineral in Pb–Zn ore deposits. In this respect, the massive presence of this mineral at some of the La Unión orebodies can indeed be considered as a peculiar and yet key paragenetic feature. In this respect, magnetite was so important in these deposits that magnetic recovery of this mineral from the froth flotation tailings was undertaken by the Peñarroya Mining and Metallurgical Company between 1959 and 1967 at La Unión; the magnetite seams at Portman Bay still represent a substantial resource that could be as large as 2.3 Mt of iron ore (Manteca *et al.*, 2014).

The Pb–Zn ore fields of La Unión and Mazarrón

The La Unión mining ore field (hosting the Emilia ore deposit)

The La Unión mining district (inactive at present) (Figs 1–3a) (Oen *et al.*, 1975; Ovejero *et al.*, 1976; Manteca & Ovejero, 1992; López-García *et al.*, 2011) is one of the most important geological, mining, and historical sites of Spain (early mining might be as old as 3000 years or even older) (UNESCO, 2015), and is an extraordinary example of the many relationships between the Miocene magmatism, tectonic and metallogenic processes in SE Spain (e.g., Oyarzun *et al.*, 1995). The La Unión orebodies, which are locally known as "mantos" (we will keep the term "manto" to follow the previous papers on the district, e.g., Oen *et al.*, 1975) are lensoid shaped, hydrothermal replacement ore deposits hosted by limestones of the Alpujárride Complex (First Manto) and marbles from

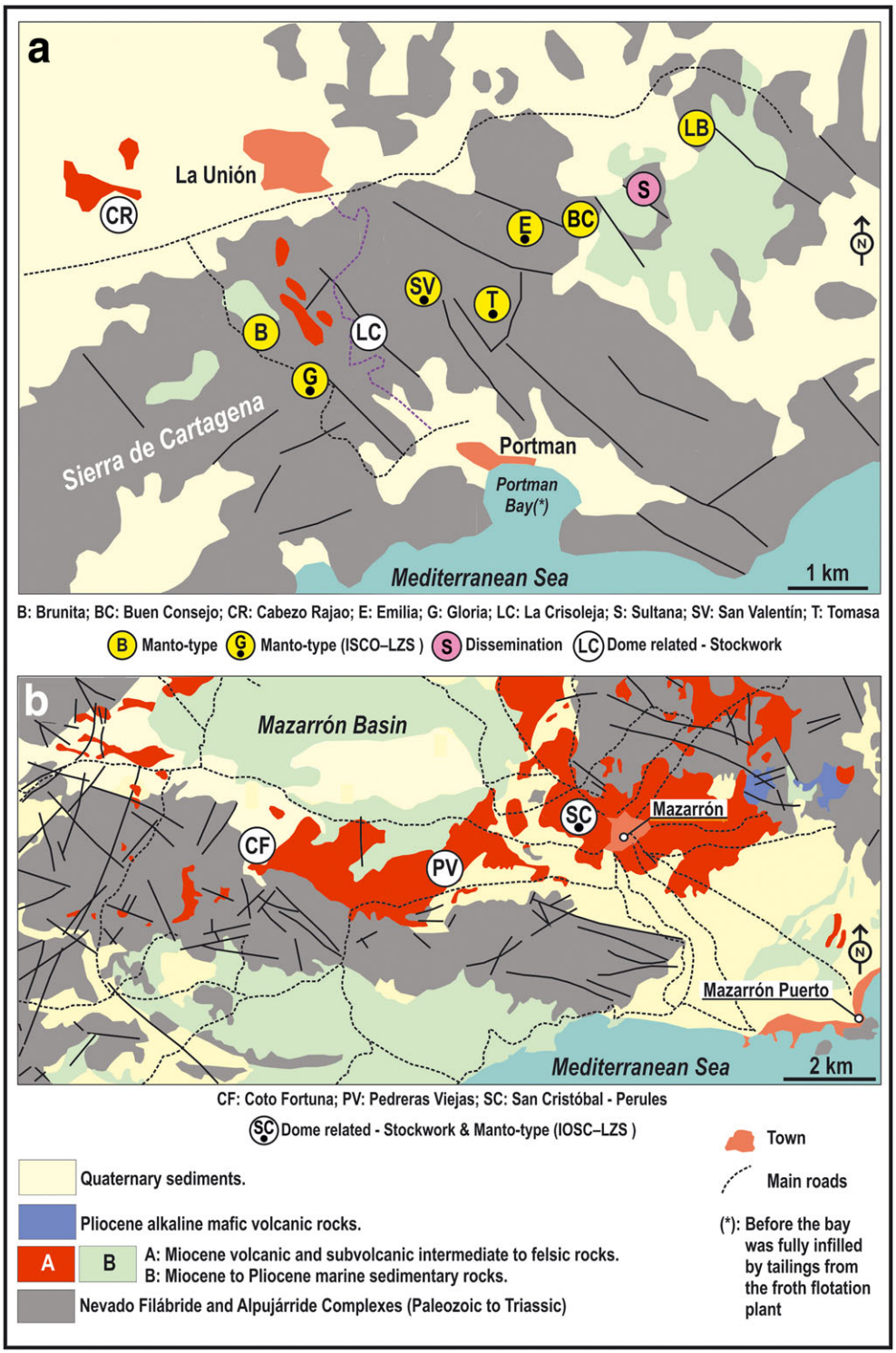

Fig. 3 Simplified geology of the (a) La Unión and (b) Mazarrón ore fields, showing location of the main mining sites. Based on Manteca and Ovejero (1992), López-García *et al.* (2011) and Oyarzun *et al.* (2011). IOSC–LZS, iron silicate, iron carbonate, iron oxide – lead and zinc sulfides.

the Nevado Filábride (Second Manto) complexes (Fig. 2a,c). These are stratabound deposits, that is, mineral deposits confined to a single stratigraphic unit (e.g., Mindat.org, 2016). Modern, open pit mining at La Unión mostly dealt with these deposits from 1953 to 1992. These are large ore bodies of up to 80 m (First Manto) to 25 m (Second Manto) thick. Pre-mining reserves were about 55 Mt (million metric tons) for the First Manto (average grades: Pb = 1.3%, Zn = 1.2%, Ag = 15 g/t) deposits and 58 Mt for the Second Manto (average grades: Pb = 1.4%, Zn = 2%, Ag = 17.5 g/t) (Manteca & Ovejero, 1992). The manto-type deposits are characterized by two distinct parageneses (P1 and P2): chlorite–sulfides–carbonate–silica (P1), and magnetite–greenalite–(minnesotaite)–siderite–sulfides–silica (P2) (IOSC–LZS); the Emilia deposit belongs to this P2 group. The IOSC–LZS paragenesis occurs only if dolerite bodies (Alpujárride Complex) or metabasic rocks (Nevado Filábride Complex) are present nearby (Fig. 2a). In this respect, the relevance of the dolerite bodies was put forward by Pavillon (1969), although their proposal was later dismissed by Oen *et al.* (1975). One of the key arguments of the latter authors was the fact that the dolerites were much older (Triassic) than the hydrothermal system (Miocene) that led to ore deposition, which precluded a causative relationship between these mafic rocks and the ore (Ridge, 1990). In this regard, perhaps both arguments have flaws: there is no need for the dolerites to be coeval with the hydrothermal system, and yet, the interaction between the hydrothermal fluids and these mafic bodies provides the most plausible explanation for the otherwise unlikely presence of greenalite at La Unión; in fact, Oen *et al.* (1975) recognized that the alteration of the iron rich dolerites may have favored formation of greenalite and magnetite. Thus, these hydrothermally altered dolerites (strong chloritization of pyroxene) could be considered as a potential source for both iron and silica. Alteration of pyroxene can lead to formation of smectite and from there to chlorite, a process involving the leaching of both iron and silica (e.g., Bettison-Varga & Mackinnon, 1997). Consequently we suggest that iron and silica removal (from the dolerites), and their subsequent transport and deposition as iron silicate (and ultimately magnetite) in the limestones (First Manto), can be explained in terms of a single hydrothermal episode affecting both rock units at the La Unión ore field. In addition, deposition of siderite does not pose a problem as the iron mobilized from the dolerites would have reacted with the Alpujárides carbonates forming siderite. The manto-type deposits are presently capped by oxidation zones thus revealing strong oxidation supergene processes that resulted in formation of gossans with a complex mineralogy of oxides, sulfates and native elements such as silver (López-García *et al.*, 1988).

The Mazarrón ore field (hosting the San Cristóbal ore deposits)

The Mazarrón Pb–(Ag)–Zn–(Fe) mining district (inactive) (López-García *et al.*, 2011; Oyarzun *et al.*, 2011; Esteban-Arispe *et al.*, 2015) is located close to the town of Mazarrón (Figs 1–3b). The site was mined, although intermittently, since Roman time, being first mined for lead and later for the alum (aluminium sulfate: alunite) during the 15th–16th Centuries, then for the alum wastes, and finally for lead, silver and zinc during the 19th and 20th Centuries (until the early 1960s). By 1927 there were 31 mines operating at San Cristóbal–Perules, with a total production of about 30,000 Mt/year with grades of 55% Pb and 1.2 to 2.0 kg/t Ag. At present the area is pervaded by huge piles of tailings extremely rich in Pb (mean = 1.24%) and Zn (mean = 0.61%), thus constituting a potential economic resource (Oyarzun *et al.*, 2011; Martín Duque *et al.*, 2015).

The volcanic activity gave rise to high-K calc-alkaline andesites, dacites and rhyodacites of Tortonian to Messinian age, that were emplaced as lavas, pyroclastic deposits, and domes within a basement constituted by the Nevado Filábride and Alpujárride complexes (Fig. 3b). The ore field hosts Pb–(Ag) –Zn–(Fe) epithermal deposits of the vein and stockwork type, and manto-type deposits at depth replacing marbles from the Nevado Filábride Complex (Figs 2a, 3b). Hydrothermal activity was triggered by the emplacement of dacitic domes of Tortonian age (9.7 ± 1.2 Ma; Esteban-Arispe *et al.*, 2015). The main deposits concentrate at San Cristóbal–Perules (adjacent to the town of Mazarrón), and the mining sites are characterized by the presence of dacitic domes (Fig. 2a) that underwent strong and pervasive advanced argillic alteration, with formation of kaolinite, alunite and silica. Main ore minerals in the veins and stockworks are Ag-rich galena, sphalerite, siderite, magnetite, and pyrite (the SC paragenesis), whereas the manto-type deposits hosts magnetite, greenalite, siderite, pyrite, galena, and sphalerite (the IOSC–LZS paragenesis) (Fig. 2a). Other sulfides in the veins and stockworks include

chalcopyrite, tetrahedrite-tennantite, arsenopyrite, cinnabar, stibnite, and berthierite; whereas supergene minerals comprise cerusite, anglesite, smithsonite, azurite and malaquite.

Magnetite, iron silicates, iron carbonates, and Pb and Zn sulfides

Until now, magnetite and iron silicates were thought to be a curious singularity restricted to some of the manto-type deposits (e.g. Emilia, San Valentín) (Fig. 3a) of the La Unión ore field (e.g. Oen *et al.,* 1975). However, the systematic study of samples from the Mazarrón (San Cristóbal deposit) ore field has shown the existence of an equivalent mineral assemblage related to concealed hydrothermal replacements in marbles belonging to the Nevado Filábride Complex (Fig. 2a), i.e. strikingly similar to the Second Manto of La Unión. However, there is scarce information about the occurrence of magnetite (and iron silicates) in the orebodies from the Mazarrón ore field and the reason why may relate to the mining and concentration procedures of the ores. Magnetite was hardly to be regarded as a welcome mineral but as an additional complexity during ore separation by gravity concentration at the end of the 19th Century–early 20th Century. During that period galena was concentrated using primitive jigs (e.g. Oyarzun *et al.,* 2011) and in this respect, a heavy mineral such as magnetite would have been a competitor for galena (both are heavy minerals). Thus, regardless of the Pb grades, there was no reason for these early miners to have sought and mined these deep magnetite rich manto-type deposits in the Nevado Filábride marble beds. In this respect, and typical of the old days: no mining – no written records.

The case was different at La Unión where the Pb–Zn–(Fe) ores were mined in modern times and therefore there is abundant and sound information. Nevertheless, as shown by the study of Esteban-Arispe *et al.* (2015), magnetite in Mazarrón is also present in the stockwork and veins (Fig. 2), although in this case is not accompanied by iron silicates such as greenalite, which seems to be a mineralogical feature restricted to the manto-type mineralization.

Mineral deposition at the replacement (P2 Manto) deposits of Emilia (La Unión) and San Cristóbal (Mazarrón) can be defined in terms of a four-stage mineral paragenesis (Fig. 4a–c), although the strong overprinting by supergene alteration mineral assemblages prevents the establishment of time–space relationships between hydrothermal alteration pulses and mineral depositional stages. The first stage is characterized by greenalite and Mn-rich (up to 3.37 wt.% MnO) siderite (Fig. 5a), which are distributed both in the groundmass and as larger crystals forming intergrowths; other mineralogical-textural features of this stage include the presence of minnesotaite and minor sulfides disseminated as minor inclusions within siderite (which is present in all the stages). A second stage involved deposition of galena, sphalerite, pyrite/marcasite and siderite (Fig. 4a,b); galena is the dominant sulfide during this second stage. Massive magnetite formed after greenalite (Figs 4d, 5a) during the third stage, and rose textures of magnetite pseudomorphs after siderite also formed (Fig. 4e); magnetite appears surrounding large idiomorphic crystals of the earlier galena. A late, fourth stage is characterized by deposition of galena, sphalerite, and pyrite/marcasite (Fig. 5b) which are accompanied by chalcedony and opal infilling fractures and cavities (Fig. 4b). The supergene oxidation of siderite and magnetite induced formation of hematite and goethite, although no specularite was observed. Minor variations are found at Mazarrón, although similar to the case of La Unión siderite and magnetite are the principal iron mineral phases. Sphalerite and pyrite (second stage) appears as disseminated grains in the carbonate-rich groundmass whereas magnetite formed after Mn-, or Zn-bearing siderite. Idiomorphic sphalerite and siderite were deposited in the late fourth stage at Mazarrón.

Magnetite mineral chemistry: results and discussion

Sampling, sample preparation, and analytical procedures

The Department of Crystallography and Mineralogy (UCM) has a large collection of samples (rocks and minerals) from La Unión; this is a site where we have traditionally conducted research and field teaching (from the late 1970s onwards), although the samples Emilia 3 and 3B (First Manto) were specifically collected for this study at the Emilia pit (Fig. 3a). Given the knowledge of some of the authors on the local ore bodies, we were able to collect representative samples suitable for a study of this kind. Our interest in Mazarrón (Fig. 3b) is more recent (from 2008 onwards) and initially came from the appalling environmental conditions in which the ore field was left. Whatever the case, we also incorporated Mazarrón to our field

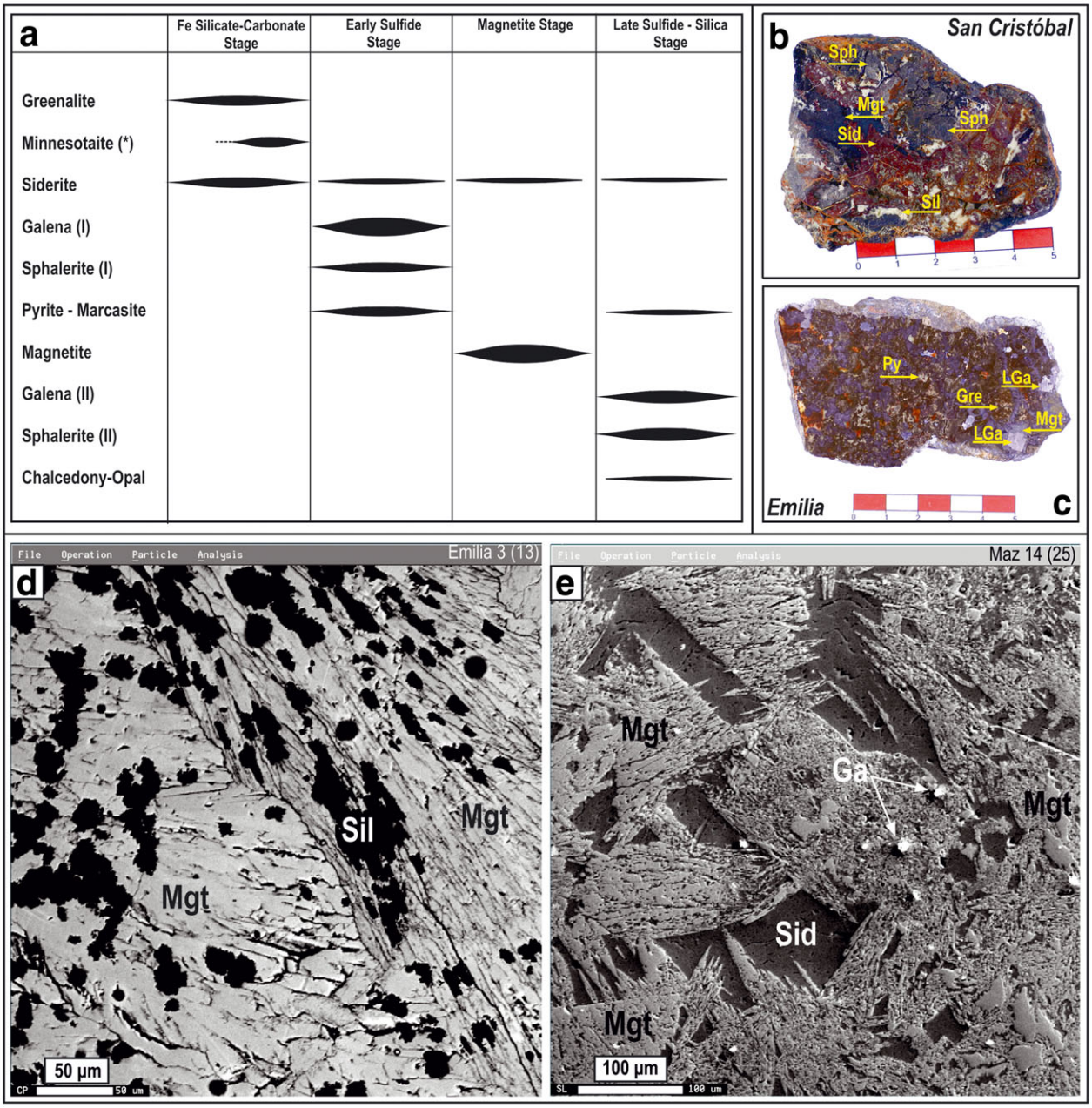

Fig. 4 Summary of a common IOSC–LZS paragenesis for San Cristóbal and Emilia (main minerals only). (a) Mineral paragenesis. (b,c) Hand specimens of IOSC–LZS ore from San Cristóbal and Emilia. (d) Back scattered electron image of magnetites from Emilia (sample Emilia 3). (e) Back scattered electron image of magnetites from San Cristóbal (sample MAZ 14). EMP, JEOL Superprobe JXA-8900 M; Gre, greenalite; LGa, late galena (II); Mgt, magnetite; Py, pyrite; Sid, siderite; Sil, silica (quartz and chalcenony); Sph, sphalerite. (*) at La Unión only.

teaching circuit, and it was only 2 years ago when we found a few samples of manto-type mineralization at San Cristóbal. These are the samples Maz-11 and Maz 14 (Maz: Mazarrón) which motivated the initiation of this study.

The samples were cut and polished at our sample preparation facilities (Department of Crystallography and Mineralogy), and carbon-coated for EPMA studies at the ICTS-National Center of Electronic Microscopy (Complutense University, Madrid, Spain) on a JEOL

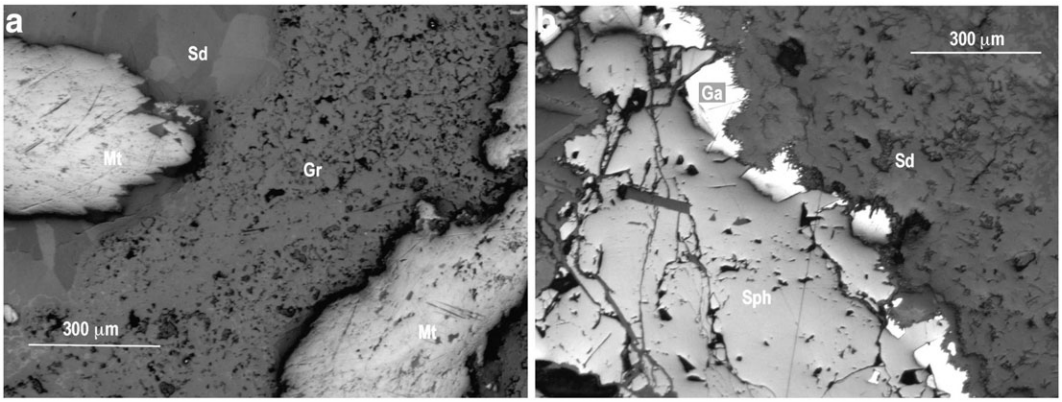

Fig. 5 Some textural features of the IOSC–LZS mineral assemblages from Emilia. (a) Magnetite (Mt) growing after greenalite (Gr) and siderite (Sd). (b) Sphalerite (Sph) and galena (Ga) in a groundmass of siderite (Sd). Mineral identification was aided by SEM–EDS (Instrument: JEOL JSM-820).

Superprobe JXA-8900 electron microprobe, which is equipped with five wavelength-dispersive spectrometers.

The analytical settings were similar to those used by Dupuis and Beaudoin (2011) for trace element microanalyses involving magnetite, that is: a 5 to 10 μm diameter beam with an acceleration voltage of 20 kV and a beam current of 100 nA. A diameter beam up to 10 μm was set to avoid overheating of grains under the selected current conditions. The analytical conditions for each element and the lower detection limits are provided in Table 1. Line overlap corrections were applied for the overlaps occurring in the analyzed spectra. The analyses were corrected for electron beam/matrix effects and instrumental drift and dead time by using the ZAF (atomic number–absorption–fluorescence) algorithm supplied with the JEOL microprobe. Also, the detection limits (DL) were calculated by the internal JEOL proprietary software from the values of the rate (count per second, cps) of net peak intensity, the rate (cps) of background intensity, the peak and background counting times (seconds), and

Table 1 Analytical conditions for the microprobe analyses of minor and trace elements in magnetites from La Unión and Mazarrón

Element	X-ray line	Analyzing crystal	Standard	Counting time (s)		Detection limit (DL) (wt%)	Nominal DL* (wt%)
				Peak	Background		
Mg	Kα	TAPH	Mg metal	20	10	0.0014–0.0015	0.001
Al	Kα	TAPH	Al metal	20	10	0.0023–0.0024	0.002
Ti	Kα	PETJ	Ti metal	20	10	0.0032–0.0033	0.003
Ca	Kα	PETJ	Kaersutite TR	20	10	0.0028–0.0029	0.003
K	Kα	PETJ	Microcline TR	20	10	0.0026–0.0027	0.003
Si	Kα	PETH	Si metal	20	10	0.0016–0.0017	0.002
V	Kα	LIF	V metal	20	10	0.0068–0.0073	0.007
Mn	Kα	LIF	MnO_2	20	10	0.0055–0.0058	0.006
Fe	Kα	LIF	Fe metal	20	10	0.0053–0.0055	0.005
Cu	Kα	LIF	Cu metal	20	10	0.0046–0.0065	0.005
Cr	Kα	LIFH	Cr metal	20	10	0.0038–0.0040	0.004
Ni	Kα	LIFH	Ni metal	20	10	0.0048–0.0050	0.004
Zn	Kα	LIFH	Zn metal	20	10	0.0066–0.0069	0.007

Instrument: JEOL Superprobe JXA-8900 M from the ITCS-National Center of Electronic Microscopy, Madrid, Spain. The analyses were performed with a 5 to 10 μm diameter beam, an acceleration voltage of 20 kV and a beam current of 100 nA. *Nominal detection limit is the figure we chose as the upper limit for the nondetects (left-censored data). Despite the fact that some of the standards chosen for the analyses are not "ideal" in consideration of the high amounts of the elements, they are well characterized, highly stoichiometric, and produce a negligible error by counting statistic during calibration; this would not be the case, if the used standards contained the desirable elements in trace amounts (Müller *et al.*, 2003).

the respective concentrations in standards. The analytical results for the studied magnetite samples are shown in Table 2.

Statistical approach

On detection limits and left-censored data

Taking into account the aforementioned DL (Table 1) and the actual results from the studied samples (Table 2) it is evident that many results fall below DL, particularly in the case of Ni and V, and to a lesser extent Cr, K, Ca, and Ti. In this respect, as indicated by Dixon (2013), environmental data often include values reported as "below detection limit." A sample is said to contain "censored data" if the only information about some of the observations is that they are below or above a specified value. These below detection limit (BDL) data (that is, left-censored data) are usually called "nondetects". In this regard, the existence of nondetects may result in some loss of information however much can be done with them at present in terms of graphical and statistical analyses (e.g., Singh & Nocerino, 2002; Dixon, 2013; He, 2013; Makvandi *et al.,* 2016; among many others). In this respect, low or very low values are as important as the larger ones to understand the statistical behavior of a given set of data. Furthermore, nondetect does not imply "0" (zero) content, but just as its name suggests, that the element concentration is BDL of the measuring instrument. That is the reason why long ago different methods were used to deal with nondetects, being among the most simple procedures those of dividing by 2 the DL (DL/2) and assigning this value to the nondetect, or by replacing it by the DL itself or zero (Singh & Nocerino, 2002). The latter however presents a serious inconvenience because it prevents the use of a logarithmic approach, which is particularly useful in geochemistry (trace elements usually have log-normal distributions; e.g., Limpert *et al.,* 2001). In fact, many distributions show important skewness, which disappears if we deal with the logarithm of the values (log x). If this is the case, we say that log x has a normal distribution, or simpler, that the distribution is log-normal (e.g., Limpert *et al.,* 2001; Martínez Coronado *et al.,* 2011).

There has been a plethora of research on these matters during the last decades, and at present there are robust estimation procedures to deal with left-censored data sets (e.g., Singh & Nocerino, 2002; Dixon, 2013; He, 2013; among many others). Thus, to model the data with appreciable nondetects (Zn, Ni, V, Cr, K, Ca, Ti, and Mg), we used robust regression on order statistics (robust ROS), with the NADA package in R (Lee, 2013). The robust ROS method (e.g., Bolks *et al.,* 2014) is based on regressing log-transformed uncensored concentrations versus their normal score (i.e., it develops a linear regression of the log-transformed concentrations on a normal probability plot using only the detected observations); the censored observations are then imputed based on this regression. If transformations are used, then the imputed values are back-transformed. Summary statistics are thus computed from the uncensored data and the imputed values (in the original scale) for the censored data. Bolks *et al.* (2014) use an arbitrary boundary at $n = 50$ (where n is the number of observations), suggesting that if $n > 50$ (we have $n = 54$) and the percent of censored data is between 50 and 80% then instead of robust the data should be dealt with maximum likelihood estimation (MLE). Given that our data population was very near to 50, we decided to try both procedures (robust and MLE). In this respect, the results in terms of mean and standard deviation were almost identical (a slight variation at 'the third decimal value'). In this respect, Dennis Helsel and Lopaka Lee, leading experts on nondetect data indicate that "MLE is notorious for producing poor estimates of the standard deviation for small datasets" (as in our case) (Helsel & Lee, 2006). They further indicate that if there were even fewer observations they would use the ROS results instead, and this is the reason we chose robust to deal with our data sets. An exception has to be made for Ni and V, which having more than 80% of nondetects generate (as indicated by R) tenuous results. Nonetheless, beyond state of the art statistical procedures, the results are telling us that these elements (Ni and V) are in very low concentrations in the studied magnetite samples. In this regard, as we explain above, very low concentrations are as important as the larger ones to understand the statistical behavior of a given set of data, and far more critical, to have a clue on the geochemical behavior of the hydrothermal system.

Software and statistical methods

To deal with the complex array of geochemical data we used the classic STATGRAPHICS Centurion XVII package and the free R software (R Core Team, 2015). R is a language and an environment for statistical

Table 2 Trace and minor element of magnetites from the San Cristóbal (MAZ 11 and 14) and Emilia (3 and 3B) deposits (Mazarrón and La Unión ore fields)

Data: wt.%	Zn	Ni	Mn	Cr	V	K	Ca	Ti	Al	Si	Mg	Fe
MAZ-11	0.012		0.051			0.047	0.012		0.083	0.068	0.004	70.254
MAZ-11	0.023		0.084		0.007	0.005	0.005		0.058	0.112		70.057
MAZ-11	0.017		0.089			0.016	0.009		0.052	0.338		67.587
MAZ-11			0.124	0.005		0.009	0.005	0.003	0.015	0.096		70.881
MAZ-11	0.018		0.085						0.017	0.087	0.007	69.915
MAZ-11	0.026		0.115			0.007			0.023	0.032		70.083
MAZ-11	0.016		0.083				0.006		0.146	0.078		70.198
MAZ-11	0.013		0.155	0.006			0.007		0.018	0.097	0.001	70.667
MAZ-14	0.052		0.073	0.004					0.040	0.029		70.155
MAZ-14	0.023		0.057						0.033	0.027	0.004	71.109
MAZ-14	0.026		0.109				0.004	0.006	0.046	0.015		70.312
MAZ-14	0.046		0.057						0.051	0.095		70.544
MAZ-14			0.042			0.033	0.009	0.006	0.016	0.417		67.055
MAZ-14	0.012		0.082						0.068	0.037		70.617
MAZ-14	0.071		0.101						0.807	0.085	0.007	69.160
MAZ-14	0.032		0.042						0.061	0.015		69.132
MAZ-14	0.019		0.051			0.019	0.004	0.006	0.027	0.234		67.023
MAZ-14	0.047		0.103				0.003		0.051	0.084		70.157
MAZ-14	0.367	0.009	0.159	0.005		0.032	0.018		0.270	0.447	0.020	66.071
MAZ-14	0.032		0.062	0.007					0.059	0.061		70.074
MAZ-14	0.017		0.071	0.005					0.056	0.072		70.239
MAZ-14	0.525		0.412			0.011	0.003		3.190	0.462	0.110	64.886
MAZ-14	0.054		0.543				0.056		0.049	0.075	0.057	66.821
MAZ-14	0.220		0.357			0.014	0.307		2.172	0.081	0.041	62.797
MAZ-14	0.017		0.156	0.006			0.020		0.102	0.016	0.011	69.676
EMILIA-3			0.043	0.004					0.026	0.074	0.001	69.778
EMILIA-3	0.010		0.038						0.017	0.649		69.465
EMILIA-3	0.014		0.051					0.005	0.064	0.096	0.005	70.785
EMILIA-3			0.042					0.007	0.029	0.062		70.030
EMILIA-3	0.011		0.030	0.006	0.008				0.006	0.043	0.002	69.982
EMILIA-3			0.019					0.010	0.013	0.011	0.001	70.579
EMILIA-3		0.006	0.049						0.025	0.100	0.002	69.987
EMILIA-3			0.019					0.004	0.036	0.042		69.828
EMILIA-3	0.009		0.072						0.029	0.123		70.513
EMILIA-3			0.055	0.012				0.004	0.019	0.098		70.279
EMILIA-3	0.012		0.035			0.003			0.030	1.652	0.002	68.236
EMILIA-3B	0.025		0.055						0.034	0.089		69.952
EMILIA-3B	0.015		0.051						0.024	0.072		69.921
EMILIA-3B			0.043				0.018		0.018	0.206		69.326
EMILIA-3B			0.034						0.020	0.107	0.003	69.884
EMILIA-3B	0.012		0.012				0.005	0.004	0.029	0.030	0.006	69.880
EMILIA-3B			0.042						0.012	0.076		70.208
EMILIA-3B	0.008		0.027		0.009		0.003		0.027	0.045	0.002	69.635
EMILIA-3B	0.008		0.026				0.004	0.005	0.023	0.069		69.085
EMILIA-3B			0.031				0.006		0.015	0.028		69.340
EMILIA-3B	0.014		0.060	0.008					0.018	0.091		69.806
EMILIA-3B			0.031				0.003		0.049	0.064	0.011	69.561
EMILIA-3B			0.042						0.019	0.711	0.005	68.881
EMILIA-3B	0.009		0.065					0.003	0.016	0.112		69.990
EMILIA-3B			0.009	0.008					0.013	0.008		70.438
EMILIA-3B			0.034	0.009					0.015	2.082		66.574
EMILIA-3B			0.029					0.005	0.016	0.081	0.002	70.406
EMILIA-3B			0.021	0.004					0.003	0.909		68.998
EMILIA-3B	0.007		0.025						0.027	0.062		69.606

Blank, not detected. See also Table 1 for instrumental conditions and sections 4.1 and 4.2 of this work.

Table 3 Geochemical data for magnetites from San Cristóbal and Emilia, and Pb–Zn deposits from elsewhere

Data: wt.%	Zn	Ni	Mn	Cr	V	K	Ca	Ti	Al	Si	Mg	Reference
San Cristóbal (n = 25)												*This work*
Mean	0.00429	0.00014	0.13052	0.00149	0.00210	0.00022	0.00045	0.00109	0.30040	0.12640	0.00019	
Standard deviation	0.00321	0.00009	0.12355	0.00087	0.00112	0.00018	0.00079	0.00054	0.74823	0.13772	0.00031	
Median	0.00334	0.00013	0.08500	0.00135	0.00196	0.00017	0.00021	0.00104	0.05200	0.08100	0.00008	
Min	0.00042	0.00002	0.04200	0.00047	0.00095	0.00001	0.00001	0.00035	0.01500	0.01500	0.00000	
Max	0.01100	0.00033	0.54300	0.00400	0.00700	0.00061	0.00300	0.00300	3.19000	0.46200	0.00100	
Emilia (n = 29)												*This work*
Mean	0.06128	0.00151	0.03759	0.00443	0.00424	0.00787	0.01767	0.00358	0.02317	0.26869	0.01055	
Standard deviation	0.11543	0.00188	0.01552	0.00245	0.00151	0.01149	0.05668	0.00198	0.01227	0.49630	0.02291	
Median	0.02300	0.00082	0.03500	0.00343	0.00381	0.00273	0.00400	0.00281	0.02000	0.08100	0.00200	
Min	0.01200	0.00031	0.00900	0.00207	0.00269	0.00068	0.00070	0.00167	0.00300	0.00800	0.00028	
Max	0.52500	0.00900	0.07200	0.01200	0.00900	0.04700	0.30700	0.01000	0.06400	2.08200	0.11000	
Pb–Zn												Dupuis and Beaudoin (2011)
Mean	0.067	0.037	0.109	0.008	0.045	na	0.006	0.039	0.061	0.015	0.019	
Median												
Min	0.059	0.034	0.066	0.008	0.011	nd	0.006	0.039	0.026	0.014	0.012	
Max	0.075	0.039	0.151	0.008	0.080	nd	0.006	0.039	0.097	0.016	0.026	
Ag-Pb–Zn												Nadoll *et al.* (2014)
Mean												
Median	0.0058	0.0085	0.0080	0.0070	0.0136	na	na	0.0154	0.0362	na	0.0129	
Min	0.0018	0.0001	0.0021	0.0006	0.0001	na	na	0.0009	0.0145	na	0.0005	
Max	0.0216	0.0152	0.0045	0.0320	0.0232	na	na	2.1900	0.4490	na	1.1500	

Zn Ni, V, Cr, K, Ca, Ti, and Mg contents for San Cristóbal and Emilia were modeled using robust regression on order statistics (robust ROS), with the NADA package in R. Magnetites from the Dupuis and Beaudoin (2011) paper were analyzed by EPMA, whereas those of Nadoll *et al.* (2014) were analyzed by EPMA and LA–ICP–MS; na, not available; nd, not detected.

computing and graphics, providing a wide variety of statistical (linear and nonlinear modeling, classical statistical tests, time-series analysis, classification, clustering, etc.) and graphical techniques. In addition, R is now widely used for discovering patterns in data sets.

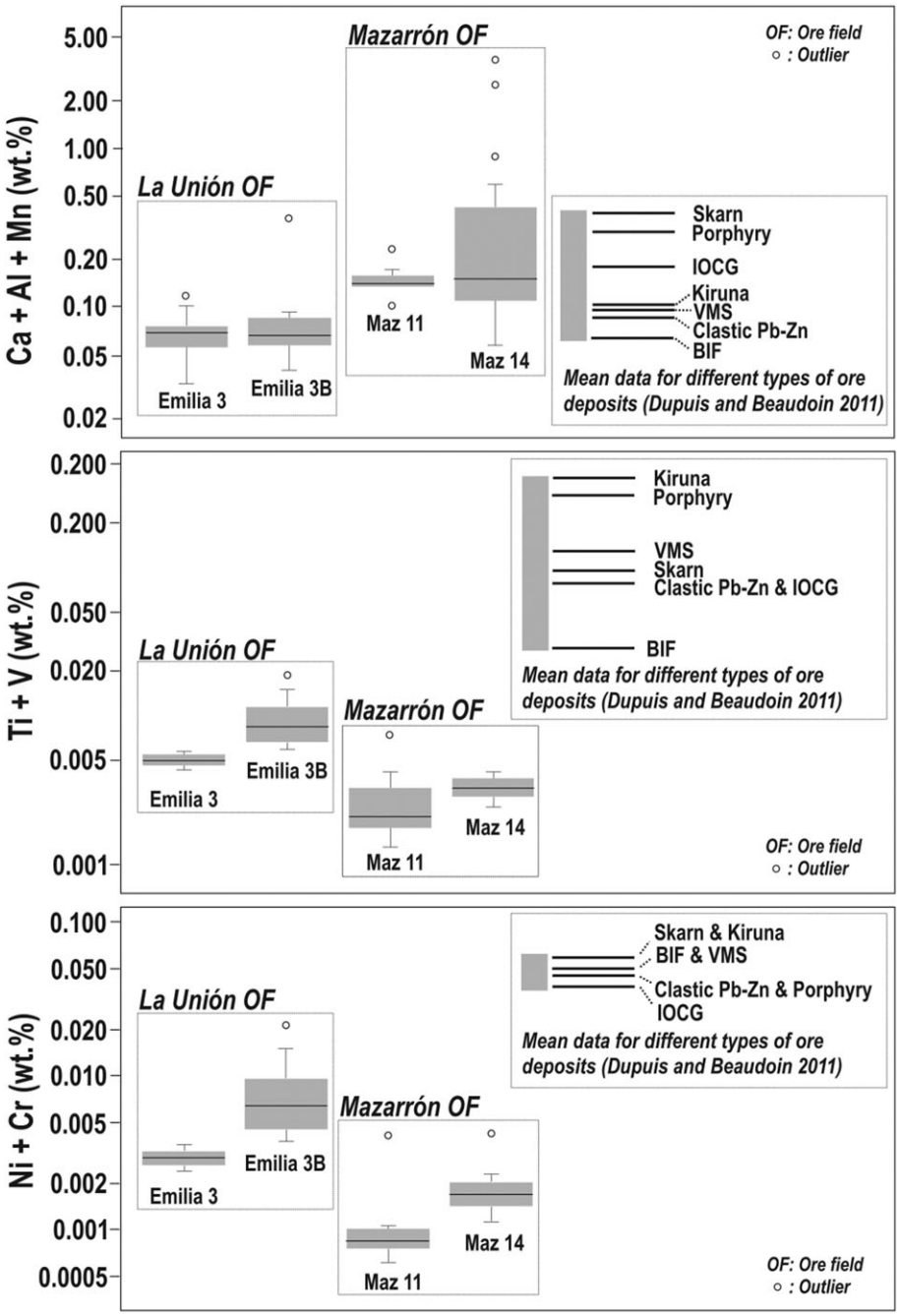

Fig. 6 Box-and-whisker plot for different data sets and elements. The central box covers the middle half of the data, extending from the lower to the upper quartile. The lines extending above and below the box (whiskers) show the location of the smallest and largest data values. The median of the data is indicated by the horizontal line within the box. IOCG, Kiruna, BIF, porphyry, skarn, VMS, hydrothermal and clastic Pb–Zn data after Dupuis and Beaudoin (2011).

We went from the simplest statistics (mean, median, standard deviation, etc) (Table 3), through box-and-whiskers graphics (which allows an easy representation of the range and median, thus offering a rapid and easy initial comparison between data sets), to principal components analysis for the identification of underlying patterns in our data (the 12 elements listed in Table 2), to highlight similarities, differences and trends (e.g., Smith, 2002; Eberly College of Science, 2015). This is particularly useful when data have been collected on the basis of a large number of variables from a single population (e.g., Smith, 2002; Eberly College of Science, 2015), which is the case of our data sets. We also performed discriminant function analysis (DFA) (e.g., Poulsen & French, 2008), a powerful statistical tool employed to determine which continuous variables discriminate between two or more naturally occurring groups. The functions are linear combinations of the input variables (the 12 elements listed in Table 2) used to separate the data into different groups. For example, this was key to determine whether the magnetites from Mazarrón (San Cristóbal) and La Unión (Emilia) corresponded to a single group or had to be understood as differentiated groups.

Magnetite from La Unión and Mazarrón

We compared our geochemical data with those of the comprehensive works of Dupuis and Beaudoin (2011) and Nadoll *et al.* (2014) (Table 3) on the mineral chemistry of magnetites from different types of ore deposits (IOCG, Kiruna, BIF, porphyry, skarn, VMS, hydrothermal and clastic Pb–Zn, etc). We first used the Dupuis and Beaudoin (2011) Ca + Al + Mn, Ti + V, and Ni + Cr parameters upon which some of their most relevant discriminant diagrams were built up. The box-and-whisker plot (Fig. 6) allows an easy comparison between the Dupuis and Beaudoin (2011) and our data sets. These elements, together with Mg can be regarded as discriminators for magnetite and show systematic variations (Nadoll *et al.*, 2014). Our data are equivalent to those of Dupuis and Beaudoin (2011) in terms of Ca + Al + Mn and lower in Ti + V and Ni + Cr (Fig. 6). On the other hand, based on data analysis and discriminant diagrams from a recent paper on trace elements in magnetite from Los Colorados (Chile) and other deposits (Knipping *et al.*, 2015), the low V (just up to 0.009% wt.% in Emilia) and Cr (just up to 0.012% wt. % in Emilia) contents of our analyzed magnetites are

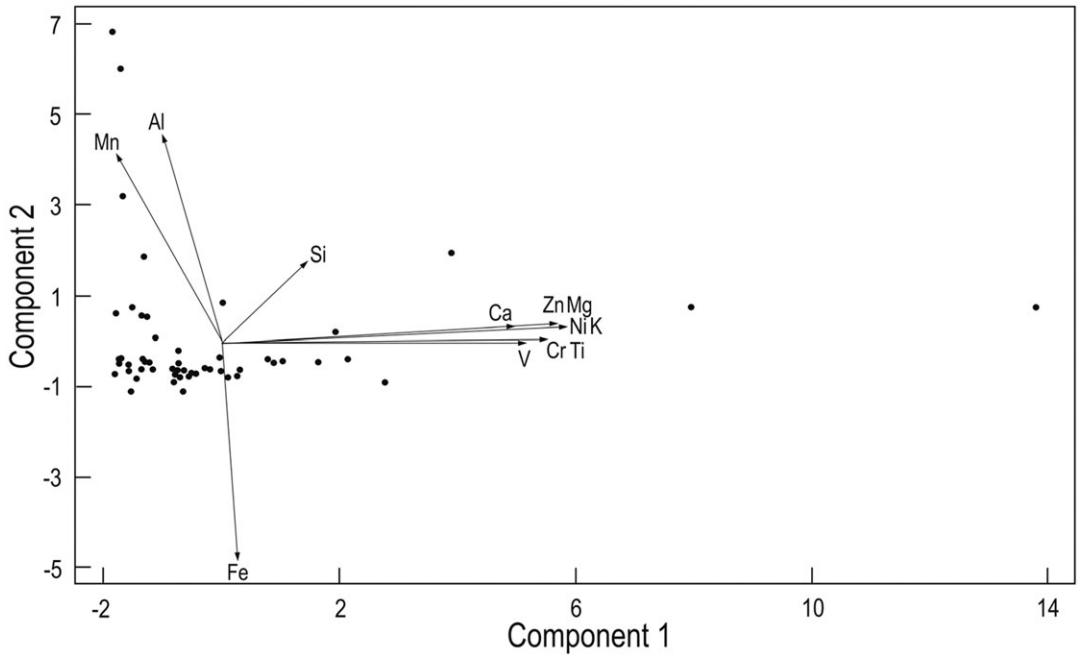

Fig. 7 PCA biplot of the scaled first and second principal components. The longer the vector the higher is the variance among the variables, whereas the angle between the vectors (cosine of the angle) approximates the correlation between the variables they represent (Kohler & Luniak, 2005). That is, the closer the angle is to 90°, or 270° the smaller the correlation; an angle of 0° or 180° reflects a correlation of 1 or −1 respectively (Kohler & Luniak, 2005). See also Table 4.

more similar to these from IOCG type deposits than those of porphyry, Kiruna or Fe–Ti–V deposits. In this respect, as indicated by Dare *et al.* (2013), hydrothermal magnetites have low concentrations for many trace elements and particularly, magnetites from the low temperature hydrothermal environments (such as that of San Cristóbal and Emilia), appear to have the lowest overall abundance of trace elements. Ti and Al can be regarded as mostly immobile under low temperatures (Nadoll *et al.*, 2014) such as those of the epithermal, shallow environment of La Unión and Mazarrón, however the same authors suggest that mobility may depend on scale, both elements being relatively mobile at the scale of meters. If we observe the mean and median data for Mazarrón and La Unión (Table 3), Mn and Al are the elements that mostly account for the Ca + Al + Mn parameter, particularly at San Cristóbal. Mn is a common ore forming metal in SE Spain (e.g., Las Herrerías) (Fig. 1), occurring also as siderite together with magnetite and iron silicates in the replacement ore bodies from La Unión and Mazarrón. This is an element typical of the epithermal environment developed in relation to volcanic centers, being also associated with Au–Ag epithermal deposits (e.g., Mosier, 1986). Besides, Dupuis and Beaudoin (2011) and Nadoll *et al.* (2014) also found elevated Mn contents in magnetites from hydrothermal Ag–Pb–Zn deposits (Table 3).

Whatever the case is for the studied elements, as indicated by Nadoll *et al.* (2014) the complex controls on the geochemistry of magnetite might become further complicated by the multiple successive stages of alteration. In this regard, given that supergene alteration practically obliterated most of the initial hydrothermal alteration assemblages at sites such as San Cristóbal, it would be difficult and mostly speculative to look for further insights regarding this matter. However, one major fact remains: despite some obvious geological differences between San Cristóbal and Emilia (Figs 2, 3) the box plots (Fig. 6) show two populations fairly consistent in their lower Ti + V and Ni + Cr as compared to the data from Dupuis and Beaudoin (2011) for other types of ore deposits.

Nonetheless, to search for the potential underlying statistical variability of the geochemical data sets from Emilia and San Cristóbal, we performed a principal component analysis (PCA) (see Fig. 7; Table 4) with the standard R command *prcomp* available through the Comprehensive R Archive Network (CRAN) (R Core Team, 2015) and double checked with STATGRAPHICS Centurion XVII.

Table 4 Principal components analysis (samples Maz 11, Maz14, Emilia 3, Emilia 3B)

Component number	Eigenvalue	Percentage of variance	Cumulative percentage
1	7.09571	59.131	59.131
2	2.27223	18.935	78.066
3	1.15088	9.591	87.657
4	0.534604	4.455	92.112
5	0.340664	2.839	94.951
6	0.227946	1.900	96.850
7	0.173773	1.448	98.298
8	0.130888	1.091	99.389
9	0.0409219	0.341	99.730
10	0.0248008	0.207	99.937
11	0.00613536	0.051	99.988
12	0.00144404	0.012	100.000
	Component 1	Component 2	Component 3
Zn	0.356192	0.049736	−0.169379
Ni	0.372425	0.0378347	−0.0513098
V	0.325761	0.00128932	0.139185
Cr	0.34795	0.00653832	0.142845
K	0.365526	0.0370434	−0.0107863
Ca	0.313179	0.0468586	−0.325826
Ti	0.349368	0.00660226	0.119778
Mg	0.358296	0.0513881	−0.178965
Al	−0.0609664	0.561845	−0.180278
Mn	−0.112731	0.516748	−0.292801
Si	0.091509	0.215409	0.787758
Fe	0.0177165	-0.600582	−0.193524

The three key principal components (i.e., with eigenvalues >1) account for 87.7% of the overall variance among the 12 variables. One of the most significant elements of the first component (Mn) is present in the mineral parageneses of Emilia and San Cristóbal (Table 4). The first component is most weighted in a positive direction on Ni (0.37), K (0.36), Zn (0.36), Mg (0.36), Cr (0.35), Ti (0.35), V (0.33), and Ca (0.31); whereas Al (0.56) and Mn (0.52) play a key role in the second component (Table 4). The most informative PCA biplot (component 1 against component 2) nicely depicts the relationships between Ni, K, Zn, Mg, Cr, Ti, V, and Ca (Fig. 7), which align following a positive trend in the X direction, whereas as Fe is roughly perpendicular to the aforementioned elements. In this regard, the closer the angle between vectors is to 90° (or 270°) the smaller the correlation between elements is, whereas an angle of 0° or 180° reflects a correlation of 1 or −1 (e.g. Kohler & Luniak, 2005). This rule would implicitly suggest that Fe does not correlate with the other elements, and the same applies to Mn, although in this case Mn the vector follows a roughly opposite

trend to that of Fe (Fig. 7); this is peculiar given that these two elements have relatively similar ionic radii: Fe^{3+} (69), Fe^{2+} (75), Mn^{3+} (72), Mn^{2+} (81) (all data in pm; Alcock, 1990), which could allow for element (Fe–Mn) substitution. On the other hand, this vector array may also reflect a more complex process such as magnetite formation after greenalite and Mn-rich siderite during ore stage 3 or metal introduction-redistribution during ore stage 4.

Another issue regarding the magnetites from San Cristóbal and Emilia concerns the degree of similarity between them. To shed some light into this matter we performed a discriminant function analysis (Fig. 8; Table 5). Our results indicate that the geochemical data sets for the magnetites from Emilia and Mazarrón separate into two well differentiated groups (80% of the samples were correctly classified) (Fig. 7), which may be revealing that subtle, and yet relevant differences appear when comparing the two ore deposits. In this regard, this is the least we could expect given that the geological setting, although very similar, is not exactly the same, with a major divergence resulting from the proximity to the igneous source. San Cristóbal is characterized by the presence of felsic domes outcrops crosscutting the carbonate rocks and schists of the Alpujárride and Nevado Filábride complexes, whereas at Emilia, the magmatic body is hidden in depth and therefore can be regarded as a distal magmatic source (Fig. 2).

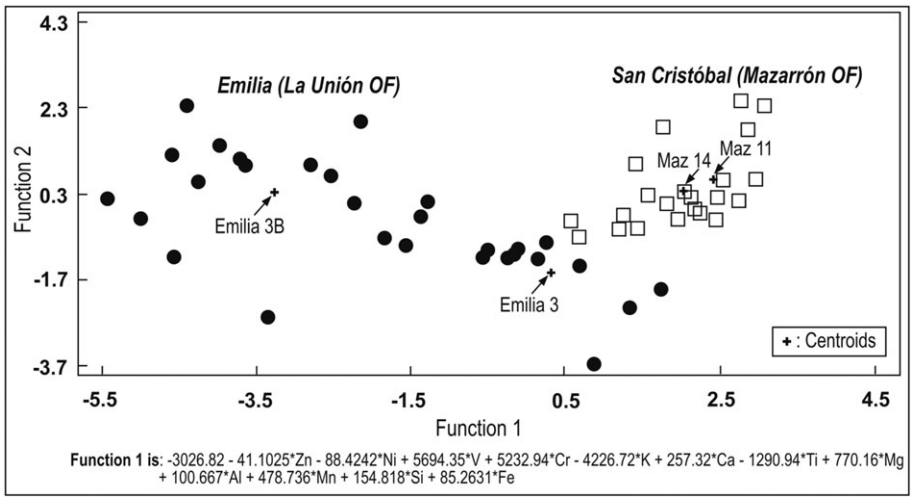

Fig. 8 Discriminant function analysis (DFA) for the four data sets from San Cristóbal (Maz 11, Maz 14) and Emilia (Emilia 3 and Emilia 3B). DFA is used here to determine which variables discriminate between naturally occurring groups. Besides, the functions are used to classify the observations into groups. If the *P*-value is <0.05 the discriminant function is statistically significant with a confidence level of 95%. In this case the *P*-value is 0.0000 for Function 1 and 0.0950 for Function 2. Thus, discrimination in groups mainly occurs along the Function 1 (X) axis. Based on the discriminant functions the percentage of cases correctly classified is 80%. We also plotted the centroids (mean discriminant scores) for each data set and Function 1. See also Table 5.

Table 5 Discriminant function analysis (samples Maz 11, Maz14, Emilia 3, Emilia 3B)

Discriminant function	Eigenvalue		Relative percentage	Canonical correlation
1	6.23097		88.00	0.92828
2	0.695824		9.39	0.63188
3	0.184805		2.61	0.39494
Functions derived	Wilks' Lambda	Chi-Square	DF	*P*-Value
1	0.0701192	119.5902	36	0.0000
2	0.50703	30.5633	22	0.1054
3	0.844021	7.6310	10	0.6648

Conclusions

From a mineralogical point of view the ore fields of Mazarrón and La Unión are probably unique among Pb–Zn–Ag deposits, having magnetite together with iron silicates (greenalite ± minnesotaite) in sufficient amounts to have developed an iron resource as in the case of the Portman Bay black sands (Manteca *et al.*, 2014). We here suggest that the leaching of iron and silica from the mafic and metamafic rocks by the hydrothermal system may have contributed to mineral deposition of iron silicates within an otherwise Fe–SiO_2 poor setting such that provided by limestones and marbles.

Contrasting geochemical results characterize the chemistry of the La Unión and Mazarrón magnetites. For example, while the Ca + Al + Mn contents are equivalent to those found in magnetites from IOCG, Kiruna, BIF, Cu porphyry, skarn, VMS, hydrothermal and clastic Pb–Zn ore deposits (Dupuis & Beaudoin, 2011; Nadoll *et al.*, 2014), the Ti + V and Ni + Cr are low. Compared to other Pb–Zn deposits, the magnetites from San Cristóbal and Emilia have similar contents in Mn and Zn. Manganese is a common metal in the epithermal environment of the late Miocene ore deposits from the Almería–Cartagena Volcanic Belt (e.g., Las Herrerías; Fig. 1). On the other hand, a late introduction of zinc (sphalerite II stage) into the ore depositional environment may account for the enrichment in this metal. Finally, the discriminant function analysis of data indicates that the magnetites from San Cristóbal and Emilia form differentiated groups, thus suggesting that the ore forming process must have been similar, but not identical, in the two ore fields. Besides, the data also reflect the chemical complexities derived from successive pulses of ore bearing fluids and the subsequent cryststallization–recrystallization of mineral phases, which no doubt must have contributed to inheritance and new additions of chemical elements. From a textural point of view, this is well exemplified by the morphological traits of magnetite formed after siderite.

Acknowledgements

This study was supported by Grant UCM 910492 (Magmatismo y Mineralizaciones en la Zona Centro-Ibérica Hercínica). We thank Dr. Sol López Andrés for her guidance with mineralogical studies at the UCM Research Support Center (CAI Técnicas Geológicas); and José Luis González Pachón for the photographic work on hand specimens. The paper benefited from the comments of Dr. A. Menzies, an anonymous reviewer, and Associate Editor S. Kojima.

References

Alcock, N. W. (1990) *Bonding and structures: structural principles in inorganic and organic chemistry*. Ellis Horwood Ltd, Hemel Hempstead, 200.

Arribas, A. and Tosdal, R. M. (1994) Isotopic composition of Pb in ore deposits of the Betic Cordillera Spain: origin and relationship to other European deposits. Econ. Geol., 89, 1074–1093.

Arribas, A. (1995) Characteristics of high-sulfidation epithermal deposits, and their relation to magmatic fluid. In Thompson, J. F. M. (ed.) *Magmas, Fluids, and Ore Deposits*, volume. 23, Mineralogical Association of Canada Ottawa Short Course, 419–454.

Arribas, A., Cunningham, C. G., Rytuba, J. J., Rye, R. O., Kelly, W. C., Podwysocki, M. H., McKee, E. H. and Tosdal, R. M. (1995) Geology, geochronology, fluid inclusions, and isotope geochemistry of the Rodalquilar gold alunite deposit, Spain. Econ. Geol., 90, 795–822.

Benito, R., López-Ruiz, J., Hertogen, J., Cebriá, J. M., Doblas, M., Oyarzun, R. and Demaiffe, D. (1999) Sr and O isotope contraints on the source and crustal contamination in the high-K calc-alkaline and shoshonitic Neogene volcanic rocks of Spain. Lithos, 46, 773–802.

Bettison-Varga, L. and Mackinnon, I. D. R. (1997) The role of randomly mixed-layered chlorite/smectite in the transformation of smectite to chlorite. Clays Clay Miner., 45, 506–516.

Bolks, A., De Wire A. and Harcum, J.B. (2014) Baseline assessment of leftcensored environmental data using R. Tech Notes 10, June 2014. Developed for the US Environmental Protection Agency by Tetra Tech, Inc., Fairfax, VA, 28 p. [Cited 31 Jul 2015.] Available from URL: https://www.bae.ncsu.edu/programs/extension/wqg/319monitoring/TechNotes/technotes10_left_censor_r.pdf.

Coleman, D. S. and Walker, J. D. (1990) Geochemistry of the Mio-Pliocene volcanic rocks from Panamint Valley, Death valley area, California. In Wernicke, B. P. (ed.) *Basin and Range Extensional Tectonics Near the Latitude of Las Vegas, Nevada*. Geological Society of America Memoir 176, Boulder, 391–411.

Crespo, E., Lillo, J., Oyarzun, R., Cubas, P. and Leal, M. (2013) The Mazarrón basin, SE Spain: A study of mineralization processes, evolving magmatic series, and geothermal activity. Internat.. Geol. Rev., 55, 1978–1990.

Dare, S.A.S., Barnes, S.J., Méric, J., Néron, A., Beaudoin, G. and Boutroy, E. (2013) The use of trace elements in Fe-oxides as provenance and petrogenetic indicators in magmatic and hydrothermal environments. 12th SGA Biennial Meeting, Proceedings 1: 256–259. [Cited 31 Jul 2015.] Available from URL: http://www.uqac.ca/labmater/publications/SGA2013_Dare.pdf

Dixon, P. (2013) Stat 505 - Environmental Statistics. Iowa State University. [Cited 31 Jan 2017.] Available from URL: http://www.public.iastate.edu/~pdixon/stat505/Chapter%2011.pdf

Doblas, M. and Oyarzun, R. (1989) Neogene extensional collapse in the western Mediterranean (Betic-Rif Alpine orogenic belt): implications for the genesis of the Gibraltar Arc and magmatic activity. Geology, 17, 430–433.

Dupuis, C. and Beaudoin, G. (2011) Discriminant diagrams for iron oxide trace element fingerprinting of mineral deposit types. Miner. Deposita, 46, 319–335.

Eberly College of Science (2015) *Applied Multivariate Statistical Analysis*. Penn State University, Pennsylvania. [Cited 31 Jan 2017.] Available from URL: https://onlinecourses.science.psu.edu/stat505/node/1

Esteban-Arispe, A., Velasco, F., Boyce, A. J., Morales-Ruano, S., Yusta, I. and Carrillo-Rosúa, J. (2015) Unconventional non-magmatic sulfur source for the Mazarrón Zn–Pb–Cu–Ag–Fe epithermal deposit (SE Spain). Ore Geol. Rev., 72, 1102–1115.

Friedrich, G., Schachner, D. and Nielsen, H. (1964) Schwefelisotopen-untersuchungen an sulfiden aus den erzvorkommen der Sierra de Cartagena in Spanien. Geochim. Cosmochim. Acta, 28, 683–686.

He, J. (2013) Mixture model based multivariate statistical analysis of multiply censored environmental data. Adv. Water Resour., 59, 15–24.

Helsel, D.R. and Lee, L.R. (2006) Analysis of environmental data with nondetects: statistical methods for censored environmental data. Joint Statistical Meetings; 2006; Seattle, Washington: American Statistical Association.

Ishihara, S. (1977) The Magnetite-series and Ilmenite-series: Granitic rocks. Mining Geol., 27, 293–305.

Ishihara, S. (2007) Origin of the Cenozoic–Mesozoic magnetite-series and ilmenite-series granitoids in East Asia. Gondowana. Res., 11, 247–260.

Knipping, J. L., Bilenker, L. D., Simon, A. C., Reich, M., Barra, F., Deditius, A. P., Wälle, M., Heinrich, C. A., Holtz, F. and Munizaga, R. (2015) Trace elements in magnetite from massive iron oxide-apatite deposits indicate a combined formation by igneous and magmatic-hydrothermal processes. Geochim. Cosmochim. Acta, 171, 15–38.

Kohler, U. and Luniak, M. (2005) Data inspection using biplots. Stata J, 5, 208–223.

Lee, L. (2013). NADA: Nondetects And Data Analysis for environmental data. R package version 1.5-6. [Cited 31 Jul 2017.] Available from URL: http://CRAN.R-project.org/package=NADA

Limpert, E., Stahel, W. A. and Abbot, M. (2001) Log-normal distributions across the sciences: keys and clues. Bio Science, 51, 341–352.

López-García, J. A., Lunar, R. and Oyarzun, R. (1988) Silver and lead mineralogy in gossan-type deposits of Sierra de Cartagena, southeast Spain. Trans. Inst. Min. Metall. (Sect. B: Appl. Earth Sci.), 97, 2–88.

López-García, J. A., Oyarzun, R., López Andrés, S. and Manteca Martínez, J. I. (2011) Scientific, educational, and environmental considerations regarding mine sites and geoheritage: A perspective from SE Spain. Geoheritage, 3, 267–275.

López-Ruiz, J. and Rodríguez-Badiola, E. (1980) La región volcánica neógena del sureste de España. Estud. Geol-Madrid, 36, 5–63.

Makvandi, S., Ghasemzadeh-Barvarz, M., Beaudoin, G., Grunsky, E. C., McClenaghan, M. B. and Duchesne, C. (2016) Principal component analysis of magnetite composition from volcanogenic massive sulfide deposits: Case studies from the Izok Lake (Nunavut, Canada) and Halfmile Lake (New Brunswick, Canada) deposits. Ore Geol. Rev., 72, 60–85.

Manteca, J. I. and Ovejero, G. (1992) Los yacimientos de Zn, Pb, Ag, Fe del distrito minero de La Unión-Cartagena, Bética oriental. In García Guinea, J., Martínez Frías, J. (eds.) *Recursos minerales de España*. CSIC Editions, Madrid, 1085–1102.

Manteca, J. I., López-García, J. A., Oyarzun, R. and Carmona, C. (2014) The beach placer iron deposit of Portman Bay, Murcia, SE Spain: the result of 33 years of tailings disposal (1957–1990) to the Mediterranean seaside. Miner. Deposita, 49, 777–783.

Martín Duque, J. F., Zapico, I., Oyarzun, R., López García, J. A. and Cubas, P. (2015) A descriptive and quantitative approach regarding erosion and development of landforms on abandoned mine tailings: New insights and environmental implications from SE Spain. Geomorphology, 239, 1–16.

Martínez Coronado, A., Oyarzun, R., Esbrí, J. M., Llanos, W. and Higueras, P. (2011) Sampling high to extremely high Hg concentrations at the Cerco de Almadenejos, Almadén mining district (Spain): The old metallurgical precinct (1794 to 1861 AD) and surrounding areas. J. Geochem. Explor., 109, 70–77.

Mindat.org (2016) Definition of strata-bound. Hudson Institute of Mineralogy. [Cited 31 Jan 2017.] Available from URL: http://www.mindat.org/glossary/strata-bound.

Morales Ruano, S., Carrillo Rosúa, F. J. and Fenoll Hach-Alí, P. (2000) Epithermal Cu–Au mineralization in the Palai–Islica deposit, Almeria, southeastern Spain: fluid-inclusion evidence for mixing of fluids as a guide to gold mineralization. Can. Mineral., 38, 553–565.

Mosier, D. L. (1986) Descriptive model of epithermal Mn. In Cox, D. P., Singer, D. A. (eds.) *Mineral deposits models*. US Geological Survey, Washington, 165–167.

Müller, A., Wiedenbeck, M., Van den Kerkhof, A. M., Kronz, A. and Simon, K. (2003) Trace elements in quartz-a combined electron microprobe, secondary ion mass spectrometry, laser-ablation ICP-MS, and cathodoluminescence study. Eur. J. Mineral., 15, 747–763.

Nadoll, P., Angerer, T., Mauk, J. L., Frenchd, D. and Walshe, J. (2014) The chemistry of hydrothermal magnetite: A review. Ore Geol. Rev., 61, 1–32.

Oen, I. S., Fernandez, J. C. and Manteca, J. I. (1975) The lead-zinc and associated ores of La Unión, Sierra de Cartagena, Spain. Econ. Geol., 70, 1259–1278.

Ovejero, G., Jacquin, J. P. and Servajean, G. (1976) Les minéralisations et leur context géologique dans la Sierra de Cartagena (Sud-Est de l'Espagne). Bull. Soc. Géol. France, 18, 619–633.

Oyarzun, R., Marquez, A., Ortega, L., Lunar, R. and Oyarzún, J. (1995) A late Miocene metallogenic province in southeast Spain: atypical Andean-type processes on a smaller scale. Trans. Instn. Min. Metall., 104, 197–202.

Oyarzun, R., Lillo, J., López-García, J. A., Esbrí, J. M., Cubas, P., Llanos, W. and Higueras, P. (2011) The Mazarrón Pb–(Ag)–Zn mining district (SE Spain) as a source of heavy metal contamination in a semiarid realm: Geochemical data from mine wastes, soils, and stream sediments. J. Geochem. Explor., 109, 113–124.

Oyarzun, R., Manteca-Martínez, J. I., López-García, J. A. and Carmona, C. (2013) An account of the events that led to full bay infilling with sulfide tailings at Portman (Spain), and the search for "black swans" in a potential land reclamation scenario. Sci. Total Environ., 454-455, 245–249.

Pavillon, M. J. (1969) Les minéralisations plombo-zincifires de Carthagène (Cordillères bétiques, Espagne). Miner. Deposita, 4, 368–385.

Poulsen, J. and French, A. (2008) Discriminant function analysis (DA). San Francisco State University. [Cited 31 Jan 2017.] Available from URL: http://userwww.sfsu.edu/efc/classes/biol710/discrim/discrim.pdf

R Core Team (2015) R: A language and environment for statistical computing. R Foundation for Statistical Computing, Vienna, Austria. [Cited 31 Jan 2017.] Available from URL http://www.R-project.org/

Ridge, J. D. (1990) *Annotated Bibliographies of Mineral Deposits in Europe: Part 2 Western and South Central Europe*. Pergamon, Oxford, 486.

Scaillet, B. (2010) Volatile destruction. Nature Geosci., 3, 456–457.

Singh, A. and Nocerino, J. (2002) Robust estimation of mean and variance using environmental data sets with below detection limit observations. Chemometr. Intell. Lab., 60, 69–86.

Smith, L.I. (2002) A tutorial on Principal Components Analysis. Computer Science, University of Otago, NZ. [Cited 31 Jan 2017.] Available from URL: http://www.cs.otago.ac.nz/cosc453/student_tutorials/principal_components.pdf

UNESCO (2015) Mining historical heritage. World Heritage Convention, Global Strategy. [Cited 31 Jan 2017.] Available from URL: http://whc.unesco.org/en/tentativelists/5139/

Viladevall, M., Font, X. and Navarro, A. (1999) Geochemical mercury survey in the Azogue Valley (Betic area, SE Spain). J. Geochem. Explor., 66, 27–35.